OAK RIDGE
NATIONAL LABORATORY
MANAGED BY UT-BATTELLE
FOR THE DEPARTMENT OF ENERGY

NFE-07-00620

Division

CRADA Final Report
For
CRADA Number NFE-07-00620

Nanocoatings for High-Efficiency Industrial and Tooling Systems

Peter Blau and Jun Qu
Oak Ridge National Laboratory

Clifton Higdon
Eaton Corporation

Prepared by
Oak Ridge National Laboratory
Oak Ridge, TN 37831
managed by
UT-BATTELE, LLC
for the
U.S. Department of Energy
under contract DE-AC05-00OR2225

Approved for
Unlimited Distribution

UT-BATTELLE
ORNL-27 (4-00)

Nanocoatings for High-Efficiency Industrial and Tooling Systems

DOE Agreement number
"**DE-FG36-06GO16054"**

CRADA Final Report
(CRADA number NFE-07-00620)

Peter J. Blau and Jun Qu
Materials Science and Technology Division
Oak Ridge National Laboratory
Oak Ridge, TN

in partnership with

Clifton Higdon
Eaton Innovation Center
Southfield, MI

Foreword

This Cooperative Research and Development Agreement (CRADA number NFE-07-00620) was effective from 1 September 2006 through 30 September 2010. Funding for the work was provided by the U.S. Department of Energy, Office of Energy Efficiency and Renewable Energy, Industrial Technologies Program (ITP), and administered by the DOE Field Office in Golden, Colorado (Mahesh Jha). The work conducted and reported in this report comprised several supporting tasks within a larger project led by Eaton Corporation [DE-FG36-06GO16054, entitled "Nanocoatings for High-Efficiency Industrial and Tooling Systems"] Participants in the ORNL portion of these activities were Peter J. Blau (Principal Investigator), Jun Qu, and Hanbing Xu, all of the Materials Science and Technology Division. A fuller description of the three-phase, four-year effort, which also involved Ames Laboratory (AL) and Greenleaf Corporation, may be found in the final report for the ITP program, which also ended officially on 30 September 2010.*

This report primarily describes friction, wear, and related characterizations that were conducted on sample materials supplied by AL and Eaton Innovation Center. It duplicates to a large extent the information that is contained within the consolidated final report that was prepared by all partners on the ITP project. The ORNL authors wish to acknowledge the contributions of the following individuals to this project.

Clifton Higdon, Eaton Corp.
Bohdan Lisowski, Eaton Corp.
Lyudmila Solovyeva, Eaton.com
Bruce Cook, Ames Laboratory
Alan Russel, Iowa State University
Jason Goldsmith, Greenleaf Corporation
Alaa Elmoursi, Eaton Corp.
Robert Milner, Eaton Corp.
Samantha Stewart, Eaton Corp.
Joel Harringa, Ames Laboratory
Vinod Sikka, ORNL (ret.)
Mahesh Jha, DOE, Golden, CO

No proprietary information has been included in this final report.

* Report number DOE/GO16054-16054-1, available online from the U.S. Department of Energy, Office of Scientific and Technical Information (OSTI) at http://www.osti.gov.

CONTENTS

1.0 Abstract

This industry-driven project was the result of a successful response by Eaton Corporation to a DOE/ITP Program industry call. It consisted of three phases in which ORNL participated. In addition to Eaton Corporation and ORNL (CRADA), the project team included Ames Laboratory, who developed the underlying concept for aluminum-magnesium-boron based nanocomposite coatings [1], and Greenleaf, a small tooling manufacturer in western Pennsylvania. This report focuses on the portion of this work that was conducted by ORNL in a CRADA with Eaton Corporation. A comprehensive final report for the entire effort, which ended in September 2010, has been prepared by Eaton Corporation.

Phase I, "Proof of Concept" ran for one year (September 1, 2006 to September 30, 2007) during which the applicability of $AlMgB_{14}$ single-phase and nanocomposite coatings on hydraulic material coupons and components as well as on tool inserts was demonstrated.. The coating processes used either plasma laser deposition (PLD) or physical vapor deposition (PVD). During Phase I, ORNL conducted laboratory-scale pin-on-disk and reciprocating pin-on-flat tests of coatings produced by PLD and PVD. Non-coated M2 tool steel was used as a baseline for comparison, and the material for the sliding counterface was Type 52100 bearing steel since it simulated the pump materials. Initial tests were run mainly in a commercial hydraulic fluid named Mobil DTE-24, but some tests were later run in a water-glycol mixture as well. A tribosystem analysis was conducted to define the operating conditions of pump components and to help develop simulative tests in Phase II.

Phase II, "Coating Process Scale-up" was intended to use scaled-up process to generate prototype parts. This involved both PLD practices at Ames Lab, and a PVD scale-up study at Eaton using its production capable equipment. There was also a limited scale-up study at Greenleaf for the tooling application. ORNL continued to conduct friction and wear tests on process variants and developed tests to better simulate the applications of interest. ORNL also employed existing lubrication models to better understand hydraulic pump frictional behavior and test results.

Phase III, "Functional Testing" focused on finalizing the strategy for commercialization of $AlMgB_{14}$ coatings for both hydraulic and tooling systems. ORNL continued to provide tribology testing and analysis support for hydraulic pump applications. It included both laboratory-scale coupon testing and the analysis of friction and wear data from full component-level tests performed at Eaton Corp. Laboratory-scale tribology test methods are used to characterize the behavior of nanocomposite coatings prior to running them in full-sized hydraulic pumps. This task also includes developing tribosystems analyses, both to provide a better understanding of the performance of coated surfaces in alternate hydraulic fluids, and to help design useful laboratory protocols. Analysis also includes modeling the lubrication conditions and identifying the physical processes by which wear and friction of the contact interface changes over time.

This final report summarizes ORNL's portion of the nanocomposite coatings development effort and presents both generated data and the analyses that were used in the course of this effort.

2.0 Statement of Objectives

The from the Eaton/ORNL CRADA Statement of Work states the following:

> "The project objective is to develop and commercialize nano-coatings of $AlMgB_{14}$ and $AlMgB_{14}$–TiB_2, as degradation-resistance materials applicable to both industrial hydraulic and tooling systems."

In addition to developing and evaluating Nano-scale Aluminum-Magnesium-Boride (NAMB) coatings to achieve superior resistance to wear and corrosion, and reduced friction for energy savings, the project also includes development of commercialization strategies to exploit technology developments.

Two applications of nanoscale coatings were selected for the ITP project of which this CRADA was a part: (1) coatings on hydraulic system components to improve seals, seats, shafts, and vanes and (2) coatings on a range of cutting inserts (carbide, cermet, and ceramic) to improve the cutting efficiency and increase tool life. Principal work on material application and testing of tool inserts was conducted by Greenleaf Inc, and those results will not be provided here.

The Oak Ridge National Laboratory portion of the collaborative work was aimed at (1) characterizing the hardness and thickness of coatings produced by partners Ames Laboratory and Eaton Corporation, (2) conducting a tribosystem analysis of proposed applications on which to base the selection and use of laboratory-scale friction and wear screening tests, (3) conducting simple coupon-type tests for pre-screening coatings and optimizing process variables, (4) developing simulative tests to evaluate coatings under conditions that mimic end use, and (5) to assist in modeling and interpreting friction and wear behavior. These are summarized in this final report.

Spanning four years, the ITP project ["Nanocoatings for High-Efficiency Industrial and Tooling Systems" Contract number, DE-FG36-06GO16054] consisted of three phases, the first two having 12 month durations, and the third with a 24 month duration:

Phase I. Proof of Concept
Phase II. Coating Process Scale-up
Phase III. Functional Testing and Commercialization

3.0 Benefits to the Funding DOE Office's Mission

The benefits of this program were described in the original, multi-partner proposal. It states the following:

> "The degradation improvement targets for the new nano-coatings [in hydraulic pumping systems] are: i) sliding friction reduction of 50%; ii) torque-to-turn reduction of 50%; iii) volumetric loss reduction over simulated lifetime of 50% (resulting in pumping efficiency improvement of 3 to 5%); and iv) start-up torque reduction of 75%. These coatings are also targeted at increasing coated cutting tool life by 50%. The technology advanced by this project is expected to result in U.S. energy saving of 31 trillion Btu/year by 2030 with associated energy cost savings of $179M/year."

Additional benefits extend beyond hydraulic pumps and tooling. In fact, as this final report is being prepared, other DOE and private industry programs are evaluating the nanocomposite coatings developed by the partners for possible use in energy-efficient transportation systems. An ITP Grand Challenge proposal to extend this approach into other novel coatings was approved in the spring of 2010.

4.0 Technical Discussion of Work Performed by All Parties

As noted in the foreword, this CRADA represents a portion of a larger project involving not only Eaton Corporation, the CRADA partner, but also Ames Laboratory and Greenleaf Corporation, who are not parties to this CRADA. The basic partition of effort was as follows:

- *Eaton Corporation* – Physical vapor deposition (PVD) NAMB coating development, process scale-up, full-sized component testing, project coordination, and hydraulic pump commercialization

- *Ames Laboratory* - NAMB coating development, surface chemistry and electron microscopy characterization, adhesion testing, pulsed laser deposition, and advice of compositional optimization.

- *Greenleaf Corporation* – Development of NAMB coatings for tool inserts used to machine titanium and other metals

- *Oak Ridge National Laboratory* – Characterization of coating hardness and thickness, characterization of friction and wear behavior, and modeling of friction based on lubrication theory.

The following sections describe ORNL contributions to the Eaton/ORNL CRADA that in turn supported the larger, multi-party ITP program.

4.1 Tribosystem Analysis

Tribosystem analysis (TSA) is an organized means by which to characterize the conductions under which materials come into contact under friction or wear-critical conditions. It comprises a problem definition that includes the geometry of contact, dimensions of parts, contact loads, sliding speeds for various operating conditions, lubricant identification and properties, operating temperatures, surface finishes, and analysis of the modes of wear and surface damage that are typically observed on the contacting parts in that tribosystem. Once a TSA is developed, it can also be used to select test methods to simulate operating conditions and screening candidate materials. Figure 1 shows the structure of the TSA form used in this project.

Using a format developed by P. Blau of ORNL, and with information provided by engineers at Eaton Corporation, TSAs were prepared for the following hydraulic pumps:

- Vane pump (vanes sliding on the internal diameter of the pump)
- Valve In Star (VIS) Motor/Pump – several interfaces within the pump section
- Piston pump – several interfaces including pistons, swash plate, and wear plate

Since the TSA contains information specific to certain of Eaton's commercial products, the above documents were shared with project team members, but are not included in this report. To support development of the VIS motor TSA, ORNL was also provided with a worn VIS motor

for examination. An analysis of the surface damage, largely from rolling contact fatigue and abrasion by trapped wear debris, was prepared and circulated to the project team members in a six page supplemental (team members only) report dated June 18, 2008.

Tribosystem Analysis (TSA) Entry Form

Project Title		Component / Application	
Manufacturer(s)		Date of TSA	
Contact person (phone / e-mail)		Problem type:	[ ] product design [ ] field problem [ ] warranty issue [ ] other:

1.0 Hardware Configurations and Materials

(Diagram or schematic)
(A) Interface location 1
(Diagram or schematic)
(B) Interface location 2
(Diagram or schematic)
(C) Interface location 3

NOTES (optional):

(A) Interface location 1 – Component descriptions

Interface (A)	Triboelement A1	Triboelement A2
1.1 General contact geometry		
1.2 Triboelement shape and general dimensions		
1.3 Current material or surface treatment		
1.4 Surface finish on the contacting area (as-finished)		
1.5 Final finishing step (on the contact area)		

(insert tables for addityional locations 2 etc.)

Figure 1(a). Tribosystem analysis form, Part 1.0 (generic).

2.0 Operating Environment
(The 'A', 'B', 'C' designations refer, respectively, to the Hardware Configuratio ns in Part 1.0)

2.1 Type of relative motion (e.g., rolling, reversed sliding, unidirectional sliding, erosion, fretting, etc.)	A) B) C)
2.2 Speed of relative motion or duty cycle	A) B) C)
2.3 Contact load, contact pressure, or pressure x velocity (PV) product on the contacting surface	A) B) C)
2.4 Temperature(s) of operation, peak /average)	A) B) C)
2.5 Lubricants of interest	A,B,C)
2.6 Lubrication supply system (drip, full flooded, vapor, if any)	A) B) C)
2.7 Characterization of third bodies (e.g., debris, grit, abrasives contaminants, if any) that appear on worn parts	
2.8 Other operating conditions relevant to the problem (corrosion, vibration, etc.)	

Figure 1 (b). Tribosystem analysis form, Part 2.0 (generic).

3.0 Problem Description

3.1 Main concern(s)	[ ] friction reduction [ ] seizure avoidance [ ] wear reduction [ ] surface damage avoidance [ ] other: _____
3.2 Which triboelement(s) is/are experiencing the problem?	A) B) C)
3.3 Dominant surface altering process(es) or wear modes for each tribo-element*	A) B) C)
3.4 Metric(s) for wear used in the application, if any (e.g., lifetime, product contamination, clearance, visual criteria, mass loss, etc)	
3.5 Problem's impact on component performance	
3.6 Cost issues or constraints on material selection	

Attach images or supporting data:

Figure 1 (c). Tribosystem analysis form, Part 3.0 (generic).

4.2 Materials and Characterization Methods

A variety of materials, ranging from steel pump vane materials to NAMB coated surfaces, were characterized and tested during the course of this project. The following methods were used:

a) Optical microscopy of surfaces and cross-sections of surfaces
b) Microindentation hardness testing
c) Micro-abrasion ball cratering for coating thickness
d) Friction and wear testing using a simple coupons
e) Friction and wear testing using parts cut from hydraulic parts
f) Full-scale hydraulic pump tests
g) Coated insert testing in machining trials of titanium and other metals
h) Scanning electron microscopy
i) X-ray Photoelectron Spectroscopy

Results of several of these are reported elsewhere, in the final report for the entire ITP project. Specifically, method (f) was conducted at Eaton Corporation facilities, method (g) was used by Greenleaf Corporation, and methods (h) and (i) were used at Ames Laboratory. Some of the latter results are included in the publications listed in 5.2. Sections 4.2.1, 4.2.2, and 4.2.3 describe the test methods performed at ORNL in support of this effort.

4.2.1 *Microindentation hardness of coated surfaces.* Traditionally, microindentation hardness tests of surfaces are obtained by slowly applying a normal load to an indenter, typically diamond, that has been ground to a specific shape. After the indenter is allowed to rest on the surface under load for 5 to 25 seconds, typically, and then removed, a microscope is used to measure the diagonal length of the remaining impression. That dimension is used to calculate the microindentation hardness number. Two common scales are the Vickers and Knoop. The differences are that the Vickers is a four-sided pyramid that is slightly sharper than the Knoop indenter which is an elongated pyramid. The latter was invented in 1938 to enable hardness testing of brittle materials in which the sharp Vickers indenter would produce undesirable cracking. The geometry of these indenters is described in ASTM E384.

Vickers hardness numbers (HV) are calculated based on load per unit facet area, but the Knoop hardness numbers (HK) are calculated from the load per unit projected area of the impression. Equations used to calculate HV and HK implicitly assume that the indenter's ideal shape is exactly replicated on the surface being tested. Due to the fact that most materials exhibit varying degrees of elastic shape recovery, depending on their elastic/plastic behavior, the HV and HK equations are not precise. However, they are commonly used without corrections for elastic recovery effects, effects that can become significant especially under low indentation loads and when the properties of materials vary with depth below the test surface. Note that so-called nanohardness is generally calculated using depth sensing rather than residual impression measurements by microscopy. These 'under-load' hardness numbers therefore should not be directly compared to microindentation hardness numbers without compensating for that difference in the measurement methodology.

The basic attributes of the Knoop and Vickers microindentation hardness test are given in Table 1. In the table, *P* is the load (in grams-force), *D* is the length of the impression diagonal (in micrometers), and *z* is the depth (in micrometers) of the impression based on the ideal indenter shape, neglecting elastic recovery. In HV testing, the diagonal length (D) is the average length of the two diagonals of the square-shaped impression; whereas in HK testing, the diagonal length (D) is that of the longer of two diagonals of the elongated diamond-shaped impression.

The form of the hardness equations is $H = C\ (P/D^2)$, where *C* is a geometric constant depending on indenter shape, hardness scale, and units.

Table 1. Comparison of Knoop and Vickers Microindentation Hardness Test Methods

	Knoop	Vickers
Constant *C* for HV or HK in units of GPa	139.6	18.19
Constant *C* for HV or HK in units of kg/mm^2	14229.	1854.4
Depth of penetration, z, relative to D	D / 30.52	D / 7.000
Depth of penetration, z, relative to HV or HK in GPa	0.387 (P/HK)$^{1/2}$	0.371 (P/HV)$^{1/2}$
Ratio of facet contact area to projected area	1.105	1.079

When a coating is applied to a surface, measurement of its indentation hardness becomes more complex. Unless the coating is so thick that it behaves as if it were a bulk material (i.e., the deposit thickness is many times the depth of indentation), the microindentation hardness number reflects the properties of a *material system* consisting of a coating atop a substrate. Factors affecting the numerical valves and repeatabililty of the results include the relative sizes of the impression depth and coating thickness, whether the coating is polyphase or single phase, the strength of the coating-substrate interface, and whether the elastic modulus and strength of the coating are less than, equal to or greater than those of the substrate. The residual stress state in the coating can also affect the resulting hardness number.

As shown in Figure 3, the response of the material system to indentation reflects a combination of substrate and coating properties. Therefore, there is no such thing as the 'microindentation hardness of a coating' if the indentation depth is greater than a substantial fraction of the coating thickness. The hardness number is that for a material A coated with a material B under the prescribed conditions. Note that elastic recovery (ER) is typically greater in the vertical direction than in the horizontal direction, further distorting the impression shape compared with the shape of the indenter that produced it. In light of the foregoing considerations, the microindentation hardness data presented in Section 4.3.1 should be viewed with caution.

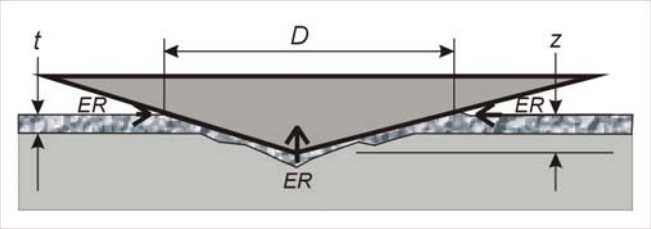

Figure 3. Indentation of a coating in which the depth of penetration (z) exceeds coating thickness (*t*). ER represents the elastic recovery of the impression once the indenter is removed.

4.2.2 *Coating thickness measurement method*. A bench-top, coating thickness measurement system based on micro-abrasion was received and set-up during this period. This equipment enables rapid and convenient measurements of coating thicknesses from approximately 0.2 to 10 μm. It is also suitable for thickness measurements on parts that have curved surfaces. A close-up view of the inclined ball resting on a test specimen is shown in Fig. 4. A few drops of a special polishing slurry is placed on the ball and it is rotated for a fixed time or number of cycles. This produces a dimple containing an inner ring of exposed substrate. Three quantities are required to measure the thickness of the coating (*t*): the ball radius *R*, the outer diameter of the dimple d_o, and the inner diameter of the exposed substrate d_i. Thus:

$$t = \frac{1}{2}\left(\sqrt{4R^2 - d_i^2} - \sqrt{4R^2 - d_o^2}\right) \qquad (1)$$

Figure 5 shows a dimple in a specimen of AlMgB14. A polished cross-section taken near the edge of the same specimen indicated a thickness of 2.2 μm, a very good agreement, considering that the coating could have been thinner nearer the edge of the specimen.

Figure 4. Motor drive unit with a 30 mm diameter ball used for micro-abrasion.

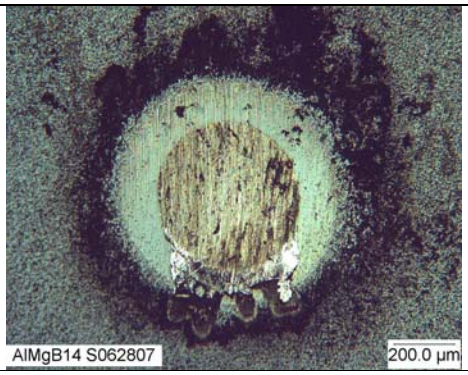

Figure 5. Dimple on a 2.51 μm-thick coating of $AlMgB_{14}$ prepared at Ames Lab.

4.2.3 *Friction and wear test methods.* The following test methods were used in the course of this effort. The first two were rather basic laboratory-scale tests, and the second two were more simulative, using sections cut from actual hydraulic pump components:

(a) a fixed ball sliding against the surface of a rotating flat specimen, referred to as the pin-on-disk (POD)
(b) a fixed ball sliding against the surface of a linearly oscillating flat specimen, referred to as the reciprocating pin-on-flat (RPOF)
(c) a vane edge sliding against the outside diameter of a circular test ring (VEOR)
(d) an oscillating section of a piston sliding against a section of the barrel.
(e) an oscillating, rolling cylinder in a round socket against cross-oriented twin-cylinders.

Tests were run either dry or lubricated with a commercial hydraulic fluid, Mobil DTE-24, or a glycol-water mixture.

Pin on disk (POD) tests were generally run using a fixed AISI 52100 steel ball (9.525 mm diameter) as the slider. The typical applied load was 10 N and the sliding speed was 0.5 m/s. The duration of sliding, reported in meters of sliding distance, was varied depending on the frictional behavior and the need for longer test times to generate measurable wear. Wear volumes of balls and flats were measured using a Wyko (Veeco) model 9100 vertical scanning interferometer. The wear volume per unit applied load and per unit sliding distance (mm^3/N-m) was reported as the wear rate.

Reciprocating pin on flat (RPOF) tests also used a fixed AISI 52100 steel ball (9.525 mm diameter) as the slider. The typical applied load was 1 or 5 N, and the sliding speed was 0.02 m/s (2.5 Hz, with a 4 mm stroke length). The duration of sliding was typically 10.2 m. Like the POD tests, RPOF tests used an interference method to map surfaces and obtain wear rates in units of (mm^3/N-m).

The vane-edge-on-ring geometry was developed in order to study the wear of the coatings against the interior surface of a vane pump. That geometry is shown in Figure 6. Steel test rings were heat treated by Eaton to attain the same hardened condition as the interior of the pump housing. A series of scoping tests in hydraulic fluid revealed that the conditions imposed were too severe to be used as a screening method for thin NAMB coatings. A drawback of the vane edge-on-ring was that lubricant could flow around the vane and therefore did not produce the kind of hydrodynamic conditions that forces vanes and bores apart in confined pump housing. A high rate of adhesive wear occurred on both vanes and rings, as well as a high level of noise and vibration. Figure 7 shows metallic flakes, characteristic of severe adhesive wear, floating in the lubricant bath.

After a number of attempts to modify the test conditions for the project, the vane edge-on-ring test method was abandoned, and no data are reported for that configuration.

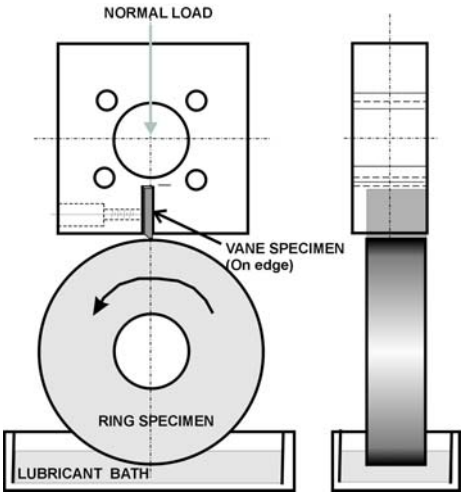

Figure 6. Vane edge of ring geometry.

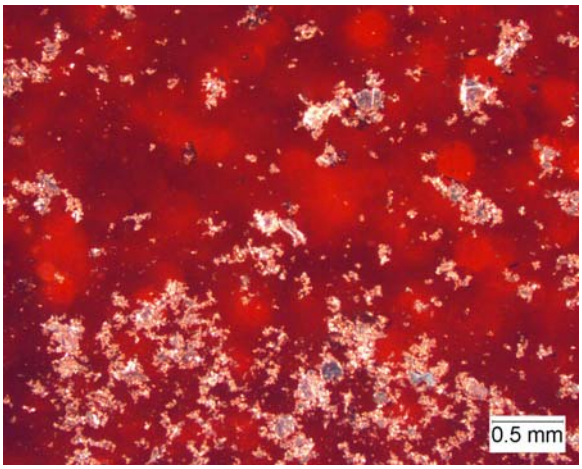

Figure 7. Metallic wear particles floating in the lubricant bath.

In addition to the POD and RPOF tests performed during Phase I, more simulative tests were developed and conducted in Phases II and III. These were based on the contact geometry and operating conditions that were listed in the TSAs for the components of interest. There were several objectives for these experiments: (a) to establish the friction and wear performance of the AMB coatings under two types of pumping fluids (Mobil DTE 24 and a water-glycol solution), (b) to determine the extent to which laboratory data would agree with pumping efficiency data from full-scale pumping tests, (c) to better understand the running-in and other transitional

behavior of various nanocomposite coating combinations, and (d) to screen variants of the coating process to determine which held most promise for commercialization.

A bench test was designed and set up at ORNL to simulate the piston-bore interface in a piston pump, as shown in Fig. 8. Load, speed, and temperature were selected to simulate the operating conditions in an actual piston pump. The resultant maximum PV value, 25000 psi*ft/min, in the reciprocating sliding test is in line with that for an actual piston pump, according to data from Eaton.

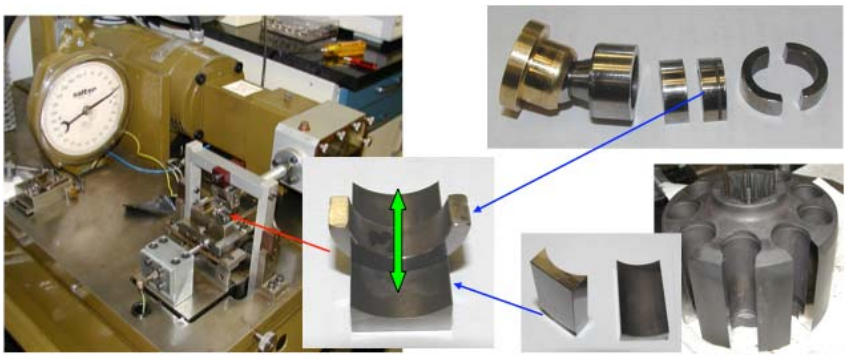

Figure 8. Setup of the bench test simulating the piston-bore interface in a piston pump.

Probably the most challenging of the simulative tests was one involving rolling combined with sliding as for the rollers the VIS motor, as shown in Fig. 9 (a). Specimen holders on a Plint model TE-77 reciprocating wear machine were modified such that the top holder was cut from the roller groove of an actual VIS. An actual roller was inserted into this groove and allowed to roll or slide back and forth on two cross-oriented cylinders to simulate the 'star' component. This setup is shown in Figure 9 (b). This bench test is intended to simulate the startup (low-rpm) operation condition that observes a reduced mechanical efficiency. Analysis of this situation is rather tricky because there are two tribocontacts of interest: (1) the rolling element in its groove, and (2) the rolling element against the 'star' (two cross-oriented cylindrical specimens in our experiments.) J. Qu of ORNL developed an analysis of the various cases in which rolling, sliding, or both occurred. For example, if the roller rolled on the bottom specimen, there would be slip between the roller and the groove. Alternatively, if the roller slides on the bottom specimen (no rolling), there might be no motion between the roller within its groove. Various combinations are possible. The challenge in controlling friction and wear is to minimize sliding unless the lubricating film thickness is great enough to avoid significant solid contact (hydrodynamic lubrication). If the component is operating under mixed, or worse, boundary lubrication, then protective coatings like AMB nanocomposites could mitigate the solid-on-solid situation, lowering wear and friction.

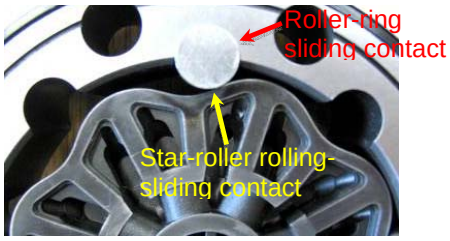

(a) Bearing interfaces in an actual VIS motor.

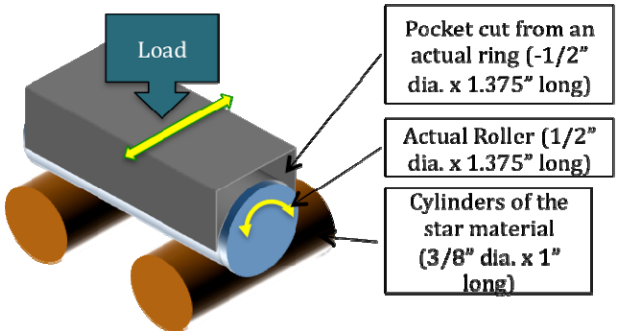

(b) Schematic of the simulated bench test.

Figure 9. Simulated bench test for VIS motor.

Observations of the experiments confirmed hypotheses about the simulation's validity and led to the development of slide-roll maps to reflect the interaction of the contact interfaces. In these maps (see, for example, Figure 10), the contact stress is plotted versus star rotation speed. Regions of acceptable and unacceptable performance, corresponding to different levels of friction coefficient, can be identified on such slide-roll maps. Low contact stress and high speed (lower left corner of the figure) combine to produce low friction and wear.

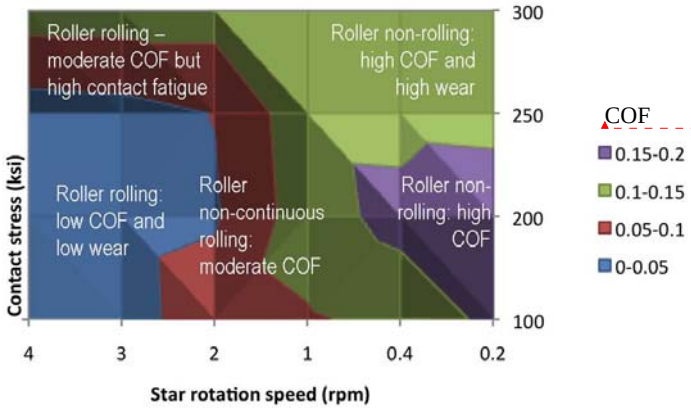

Figure 10. Slide-roll map developed at ORNL.

Formatted: Font: 11 pt

Tooling applications. A limited number of high-temperature pin-on-disk tests (400 ^{o}C and 800 ^{o}C) were performed on tungsten carbide and coated tungsten carbide (WC) to address a cutting tool application (cutting of aerospace Ti alloys). Test disks for these studies were provided by Greenleaf Corporation. Early tests of WC disks against pins of titanium alloy Ti-6Al-4V at 800 ^{o}C (load 60.33 N, speed 0.9 m/s, in air) produced severe degradation and macroscopic delamination of the surface of disk specimens, largely due to oxidation (see Figure 11(a)). The nanocomposite coating protected the surface (Fig. 11(b)). It is concluded that the main benefit of coatings is to prevent oxidation of the WC under temperatures that are generated by the cutting process.

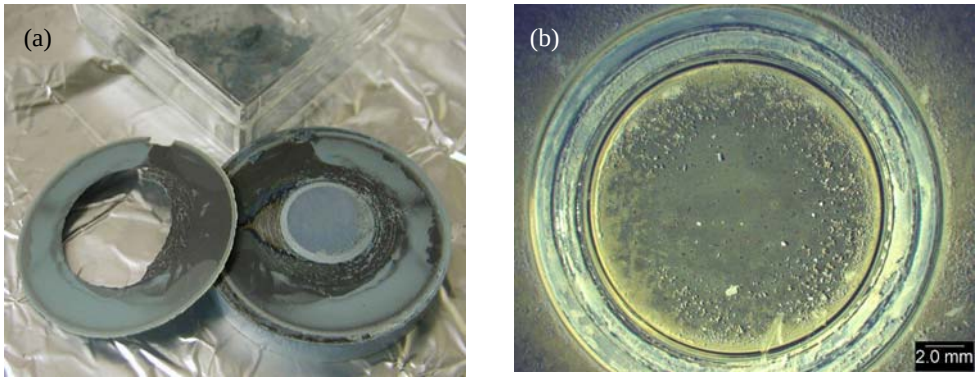

Figure 11. (a) The entire top surface of the uncoated WC-Co disk specimen delaminated during testing at 800^{o} C in air. (b) Although the Ti pin wore through the AMB, the non-worn areas protected the disk from atmospheric attack under the same conditions.

4.3 Test Data and Results

4.3.1 *Coating Thickness and Hardness Measurements*. The thickness of coatings was measured by Eaton Corporation by polished cross-sections and by ORNL using a ball-cratering method. Microindentation hardness numbers, subject to the limitations discussed in 4.2.1, were measured using the Knoop scale at 100 grams-force applied load. Surface roughness of the specimens, reported as an arithmetic average (Ra), was measured using a stylus profiling instrument. Results of these measurements are summarized in Table 2, along with ratios of parameters:

t / Ra = ratio of coating thickness to roughness
z / t = ratio of indentation penetration depth to coating thickness

The (t/Ra) ratio indicates how much thicker or thinner the coating was relative to the as-coated microgeometry of the surface. Low (t/Ra) ratios suggest that the coating follows the surface finish and might be prone to fail at the profile's peaks. The (z/t) ratio suggests the degree to which the properties of the substrate would influence the apparent hardness of the coating-

substrate system (anvil effect). This latter quantity varied from about 0.19-0.75, with larger values indicating that the substrate properties had greater influence on the hardness number.

Table 2. Consolidated Thickness, Roughness, and Hardness Data for Nanocoatings.

Specimen	t (μm)	R_a (μm)	t/R_a	HK (GPa, 100 g-f)	z (μm)	z/t
M2 steel vane (no ctg)	n/a	0.18	n/a	9.4	1.26	
DLC + TiN interlayer	1.2	0.16	7.5	17.2	0.93	0.78
EB1065-HT $AlMgB_{14}$-TiB_2	3.8	0.16	23.8	29.1	0.72	0.19
DLC2	2.5	0.18	13.9	18.7	0.89	0.36
EB1071-LT $AlMgB_{14}$-TiB_2	3.0	0.17	17.6	19.8	0.87	0.29
EB1101 Ti-TiB_2	2.4	0.19	12.6	21.2	0.84	0.35
EB1106 $AlMgB_{14}$-TiB_2+high-C	3.1	0.21	14.8	11.0	1.17	0.38
EB1108 $AlMgB_{14}$-TiB_2+C, LT	3.8	0.20	19.0	11.1	1.16	0.31
EB1112 $AlMgB_{14}$-TiB_2+C-target	3.4	0.18	18.9	18.9	0.89	0.26
EB1114 $AlMgB_{14}$-TiB_2+C	2.5	0.15	16.7	10.3	1.21	0.48
EB1115 $AlMgB_{14}$-TiB_2+low-C	2.4	0.15	16.0	19.5	0.88	0.37
EB1107-HT $AlMgB_{14}$-TiB_2	2.6	0.18	14.4	25.2	0.77	0.30
EB1121-LT $AlMgB_{14}$-TiB_2	1.2	0.14	8.6	13.2	1.07	0.89
EB1124 $AlMgB_{14}$-TiB_2+C	3.2	0.16	20.0	12.8	1.08	0.34
EB1124 $AlMgB_{14}$-TiB_2+C on 52100 steel	2.7	0.13	20.8	16.4	0.96	0.35
EB1166 $AlMgB_{14}$-TiB_2+C on A2 steel	4.3	0.23	18.7	15.1	1.00	0.23
EB1166 $AlMgB_{14}$-TiB_2+C on M2 steel		0.17		15.1	1.00	
EB1174 $AlMgB_{14}$-TiB_2+C	4.5	0.14	32.1	13.3	1.06	0.24
EB1176 $AlMgB_{14}$-TiB_2+C	4.1	0.14	29.3	12.0	1.12	0.27

4.3.2 *Pin-on-Disk Tribotest Results.*

Pin-on-disk friction and wear tests were conducted over a four-year period, and the results have been consolidated in Table 3, for Mobil DTE-24 test fluid, and Table 4 for water-glycol test fluid. In this and subsequent tables, the 'vane' material was used for the rotating disk specimen and the pin was 52100 steel.

Final friction coefficients at the ends of the tests, as reported in Tables 3 and 4 did not reflect the frictional variations observed during the tests. Sometimes, due to initial abrasion from the harder of the coated surfaces, the friction began higher and then settled to a lower value as the surfaces wore-in. Examples of friction coefficient versus sliding distance behavior are shown in Figure 12.

Table 3. Pin-on-Disk Tribotest Results for Specimens Tested in Mobil DTE-24.

Vane Material	Sliding Dist. (m)	Final COF	WR of Vane (mm^3/N-m)	Wear Rate of Ball (mm^3/N-m)
M2 steel vane	5,400	0.58	12.0x10-8	239x10-8
DLC on M2 (w/o TiN)	10,800	0.1	n/m*	0.6x10-8
DLC on M2 (w/ TiN)	10,800	0.14	n/m*	1.1x10-8
AlMgB14-TiB2 on M2 (EB1065)	10,800	0.14	n/m*	1.0x10-8
AlMgB14-TiB2 on M2 (EB1071)	10,800	0.08	n/m*	2.9x10-8
TiB2 on M2 (EB1101, vane #2)	11,100	0.07	n/m*	2.0x10-8
AlMgB14-TiB2+C on A2 (EB1166)	32,400	0.02	4.0x10-8	1.2x10-8
AlMgB14-TiB2+C on M2 (EB1166)	32,400	0.02	3.0x10-8	0.9x10-8
AlMgB14-TiB2+C (EB1174)	32,400	0.03	4.4x10-8	0.1x10-8
AlMgB14-TiB2+C (EB1176)	32,400	0.05	3.0x10-8	0.1x10-8
AlMgB14-TiB2+C (1186)	32,400*	0.04	7.6x10-8	0.80x10-8
AlMgB14-TiB2+C (1187)	32,400*	0.06	5.0x10-8	0.15x10-8
AlMgB14-TiB2+C (1188)	32,400	0.06	4.0x10-8	0.32x10-8
AlMgB14-TiB2+C (1189)	32,400	0.04	4.6x10-8	0.43x10-8
AlMgB14-TiB2+C (1190)	32,400	0.07	3.8x10-8	0.15x10-8
AlMgB14-TiB2+C (1191)	32,400	0.07	4.3x10-8	0.15x10-8
AlMgB14-TiB2+C (1192)	32,400	0.07	4.5x10-8	0.05x10-8

* n/m = not measurable (<1 x 10^{-7}), WR = wear rate, COF = coefficient of friction

Table 4. Pin-on-Disk Tribotest Results for Specimens Tested in Water/Glycol*

Vane Material	**Sliding Dist. (m)**	**Final COF**	**WR of vane (mm^3/N-m)**	**WR of ball (mm^3/N-m)**
M2 steel vane	1000	0.24	2.2x10-7	13.9x10-7
M2 steel vane	1000	0.61	3.6x10-7	19.5x10-7
DLC (w/ TiN)	1000	0.11	*n/m**	5.5x10-7
DLC (w/o TiN)	1000	0.1	(<0.5x10-7)	2.5x10-7
AlMgB14-TiB2 (EB1065)	1000	0.1		0.9x10-7
AlMgB14-TiB2 (EB1071A)	5400	0.02	0.8x10-7	0.6x10-7
AlMgB14-TiB2 (EB1071B)	5400	0.03	0.9x10-7	0.3x10-7
AlMgB14-TiB2 (EB1071B2)	5400	0.05	0.5x10-7	0.5x10-7
DLC (w/ TiN)	10800	0.04	*n/m**	0.3x10-7
AlMgB14-TiB2+lowC (EB1115)	5400	0.11	<0.5x10-7	0.5x10-7
AlMgB14-TiB2+C (EB1114)	5400	0.1	1.7x10-7	0.1x10-7
AlMgB14-TiB2+C-LT (EB1108)	5400	0.12	1.8x10-7	0.1x10-7
AlMgB14-TiB2+C-target (EB1112)	5400	0.1	<0.5x10-7	0.8x10-7
Ti-TiB2 (EB1101) (vane 1)	5400	0.24	0.7x10-7	0.5x10-7
Ti-TiB2 (EB1101) (vane 2)	5400	0.04	*n/m**	0.8x10-7

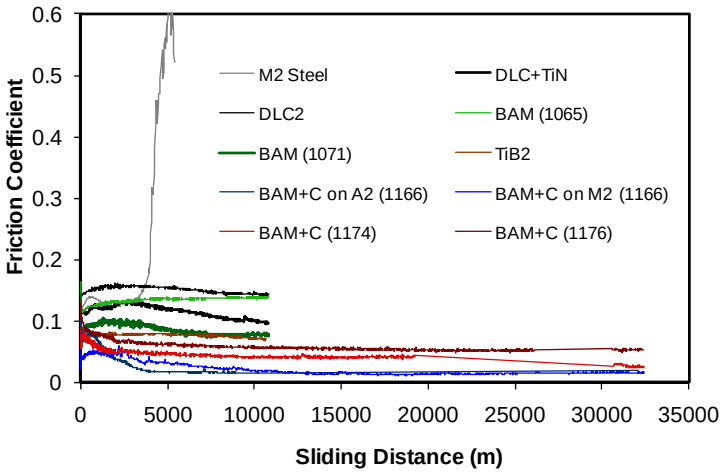

Figure 12. Friction coefficients exhibited running-in behavior. The lowest final fricrtion coefficients were observed with long tests. Friction of the uncoated M2 steel rose quickly an the test was terminated.

4.3.3 *Reciprocating Pin on Flat Tribotest Results*.

Table 5 shows a summary of reciprocating pin-on-flat tests. Since the reciprocating motion disturbs the lubricant regime and did not simulate the constant sliding direction in pumps, these tests did not prove to be as useful as the pin-on-disk results presented above. Therefore only a modest matrix was completed. Nevertheless, the results follow.

Table 5. Reciprocating Pin-on-Flat Tribotest Results for Dry Conditions and for Lubrication with Mobile DTE-24

	Lubrication conditions and test load			Vane WR	Pin WR
	(none)	(none)	DTE-24	(none)	(none)
	Load = 1 N	Load = 5 N	Load = 5 N	(mm^3/N-m)	(mm^3/N-m)
M2 steel vane	0.67	0.56	0.14	n/m*	3.57x10-5
Ames S062807	0.7		0.18	n/m*	11.0x10-5
Ames S072607	0.20 ~ 0.80		0.13	1.61x10-5	0.52x10-5
Ames S080907	0.21~ 0.72			0.55x10-5	3.96x10-5
Ames S091007	0.8			1.17x10-5	1.05x10-5
Ames S102307	0.81			1.03x10-5	0.54x10-5
Ames S111307	0.74			0.74x10-5	0.87x10-5
Eaton EB1038A	0.78			10.1x10-5	1.50x10-5
Eaton EB1039A	0.83			4.26x10-5	0.26x10-5
Eaton EB1065A	0.84			n/m*	1.66x10-5
Eaton DLC	0.21	0.18	0.12	n/m*	0.28x10-5
Ames SAM-L-TB-M1	0.16 ~ 0.98			1.39x10-5	0.21x10-5
Ames SAM-TB70-TC-M1	0.17~ 1.12			0.60x10-5	0.27x10-5

4.3.4 *Results from Bench Tests Developed to Simulate Components in Piston Pumps*

Comparative friction tests for uncoated, DLC-coated, and BAMC-coated pistons against the uncoated bores were carried out in the full temperature range and results are shown in Fig. 13. Apparently, the BAMC coating exhibited the best frictional behavior with friction reduction up to 60% compared to the uncoated production piston. The DLC coating, however, produced mixed results. Twenty-four hours wear tests were conducted to examine the long-term friction performance and coating durability. The friction coefficient for the BAMC-coated piston produced consistently lower friction than the uncoated and DLC-coated ones along the test. The BAMC coating had no measurable wear but mild polishing after the 24-hr wear test.

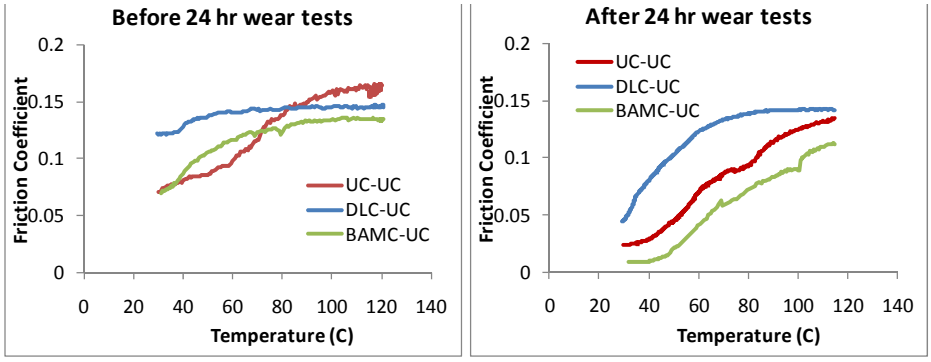

Figure 13. BAMC-coated piston produced substantial lower friction compared with the uncoated and DLC-coated pistons over the full range of pump operation temperatures.

4.3.5 *Results from Bench Tests Developed to Simulate Components in VIS Motors*

VIS-simulative rolling-sliding bench tests were carried out on three different material combinations as follows:

- UC-UC-UC: uncoated steel ring, roller, and star,
- UC-BAMC-BAMC: uncoated ring, BAMC-coated roller, and BAMC-coated star,
- UC-DLC-BAMC: uncoated ring, DLC-coated roller, and BAMC-coated star.

A series of contact pressure and sliding speed combinations were used to cover the full range of the startup operating condition for a VIS motor. Tests were conducted at room temperature and lubricated by Mobil DTE-24™ oil.

The combination of uncoated steel ring, DLC-coated roller, and BAMC-coated pins (star material) showed significantly reduced traction (friction) compared to the conventional uncoated version, as shown in Table 6 and Figs. 14. In Table 6 the rolling 'yes' or 'no' refers to whether the roller shown in Fig. 9(b) was observed to roll during the test. Results suggest that the combination of DLC and BAMC nano-coatings can substantially improve the startup efficiency for the VIS motor.

The self-mated BAMC contact, however, showed little benefit, and even underperformed the uncoated set under certain conditions (see Fig. 14). This confirms our prediction that similar materials rubbing each other more likely causes friction and wear issues due to high adhesion at the interface.

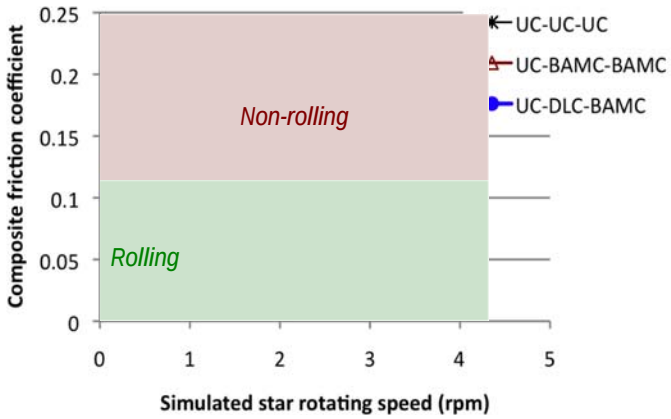

(a) Under a constant load of 10 N (109 psi)

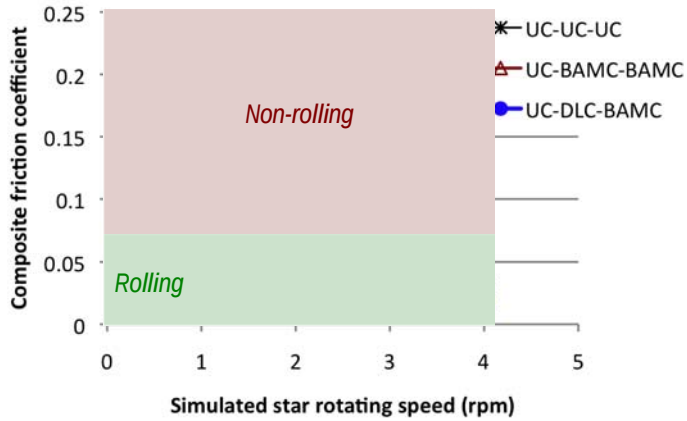

(b) Under a constant load of 60 N (198 psi)

Figure 14. Roller rolling status versus composite friction coefficient.

Table 6. Summary of results for the pin-on-twin bench test for VIS motors.

Ring-Roller-Pin Materials		Uncoated-uncoated-uncoated		Uncoated-BAMC-BAMC		Uncoated-DLC-BAMC	
Load	Slid-Freq (Star w)	Roller rolling?	Comp. COF	Rolling?	COF	Rolling?	COF
10 N (109 ksi)	1 Hz (4 rpm)	Yes	0.028	Yes	0.032	Yes	0.027
	0.75 Hz (3 rpm)	Yes	0.033	Yes	0.027	Yes	0.021
	0.5 Hz (2 rpm)	Yes	0.073	No	0.125	Yes	0.028
	0.25 Hz (1 rpm)	Yes after re-aligned	0.095	No	0.129	Yes	0.045
	0.1 Hz (0.4 rpm)	Yes after re-aligned	0.115	No	0.130	No	0.104
	0.05 Hz (0.2 rpm)	Non-continuous	0.163	No	0.130	No	0.101
60 N (198 ksi)	1 Hz (4 rpm)	Yes	0.034	Yes	0.022	Yes	0.018
	0.75 Hz (3 rpm)	Yes	0.035	Yes	0.026	Yes	0.015
	0.5 Hz (2 rpm)	Yes	0.045	No	0.121	Yes	0.021
	0.25 Hz (1 rpm)	Non-continuous	0.127	No	0.117	Yes	0.046
	0.1 Hz (0.4 rpm)	No	0.168	No	0.117	No	0.084
	0.05 Hz (0.2 rpm)	No	0.212	No	0.116	No	0.079
120 N (249 ksi)	1 Hz (4 rpm)	Yes	0.027	Yes	0.042	Yes	0.023
	0.75 Hz (3 rpm)	Yes	0.033	Yes	0.052	Yes	0.022
	0.5 Hz (2 rpm)	Yes	0.051	No	0.116	Yes	0.033
	0.25 Hz (1 rpm)	No	0.133	No	0.113	Yes	0.056
	0.1 Hz (0.4 rpm)	*Not tested*		*Not tested*		No	0.082
	0.05 Hz (0.2 rpm)	No	0.124	No	0.112	No	0.081
200 N (295 ksi)	1 Hz (4 rpm)	Stopped rolling after 20s	0.069→0.123	No	0.115	Yes	0.024
	0.75 Hz (3 rpm)	*Not tested*		*Not tested*		Yes	0.031
	0.5 Hz (2 rpm)	*Not tested*		*Not tested*		Yes	0.046
	0.25 Hz (1 rpm)	*Not tested*		*Not tested*		No	0.084
	0.05 Hz (0.2 rpm)	*Not tested*		*Not tested*		No	0.083

4.3.5 *Lubricant Film Thickness Calculation and Analysis*

Lubrication modeling was conducted to gain mechanistic understanding of the friction and wear behavior for the bearing components in actual hydraulic systems to aid the coating development.

There are three lubrication regimes, elastohydrodynamic (EHL), boundary (BL), and mixed (ML) lubrication, as illustrated by the Stribeck curve in Fig. 15. Under EHL (low load and/or high velocity), the two solid surfaces are totally separated by a liquid lubricant film, resulting in a low friction and virtually no wear. The friction coefficient is entirely controlled by the lubricant viscosity and pressure-viscosity coefficient. Under boundary lubrication (high load and/or low velocity), the two solid surfaces are in contact and usually generate higher friction and more wear. The friction behavior is determined by the mechanical and thermal properties of both the solid and liquid in a synergistic effect. The ML falls in between EHL and BL and, because of the nature of a transition regime, the associated friction and wear are sensitive to the operation condition and material properties.

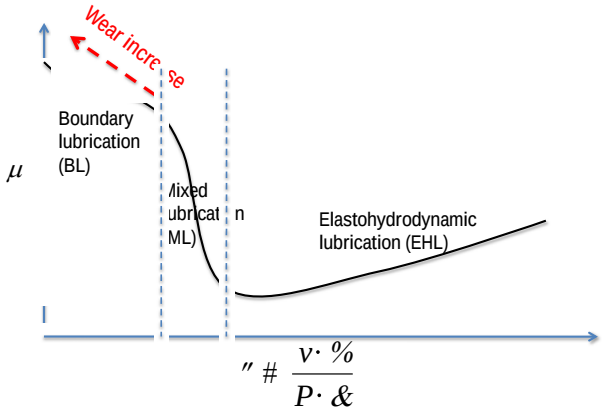

Figure 15. Stribeck curve illustrating the three lubrication regimes.

The ratio (λ) between the lubricant film thickness (h) and the composite roughness (σ) is usually used to determine the lubrication regime, as shown below:

$$\lambda = \frac{h}{\sigma} \qquad \begin{cases} \lambda \le 1, & BL \\ 1 < \lambda \le 4, & ML \\ \lambda > 4, & EHL \end{cases} \tag{1}$$

The composite roughness is defined as $\sigma = \sqrt{\sigma_1^2 + \sigma_2^2}$, where σ_1 and σ_2 are the RMS roughness of the two contact surfaces, $\sigma_1 = R_{q,1}$ and $\sigma_2 = R_{q,2}$.

The lubricant film thickness can be calculated using the Hamrock and Dowson formulas [2]. For example, Equations (2) and (3) compute the minimum film thickness in the contact area for a Hertzian point contact and a Hertzian line contact, respectively.

$$h_{point} = \frac{3.63U^{0.68}G^{0.49}}{W^{0.073}}[1 - e^{-0.68\kappa}] \cdot R_x \tag{2}$$

$$h_{line} = \frac{2.65U^{0.7}G^{0.54}}{W^{0.13}} \cdot R_x \tag{3}$$

where W, U, G, κ, R_x, R_y E' are dimensionless parameters as expressed below.

Load: $W = \dfrac{w}{R_x^2 \cdot E'}$

Speed: $U = \dfrac{\eta_0 \cdot (u_1 + u_2)}{2R_x \cdot E'}$

Material: $G = \alpha \cdot E'$

Ellipticity: $\kappa = 1.0339\left(\frac{R_y}{R_x}\right)^{0.636}$

Effective Radii: $R_x = \frac{R_{1x} \cdot R_{2x}}{R_{1x} + R_{2x}}$, $R_y = \frac{R_{1y} \cdot R_{2y}}{R_{1y} + R_{2y}}$

Composite modulus of elasticity: $E' = \frac{2}{\frac{1-\nu_1^2}{E_1} + \frac{1-\nu_2^2}{E_2}}$

where

w – Normal load
η_0 – Atmospheric absolute viscosity
α – Viscosity-pressure coefficient
u_1, u_2 – Surface velocities of the two surfaces in x direction
R_{1x}, R_{2x} – Radii of the two surfaces in x direction
R_{1y}, R_{2y} – Radii of the two surfaces in y direction
E_1, E_2 – Modula of elasticity of the two surfaces
ν_1, ν_2 – Poisson ratios of the two surfaces

Case study – analysis of the low start-up efficiency for VIS motors

According to the field experience at Eaton Corp., the VIS motor mechanical efficiency has strong relation to the motor rotation speed and drops linearly when the speed is below 4 rpm (at start-up), as shown in Fig. 16. Lubrication modeling was conducted at ORNL to understand the mechanism and provide potential solutions.

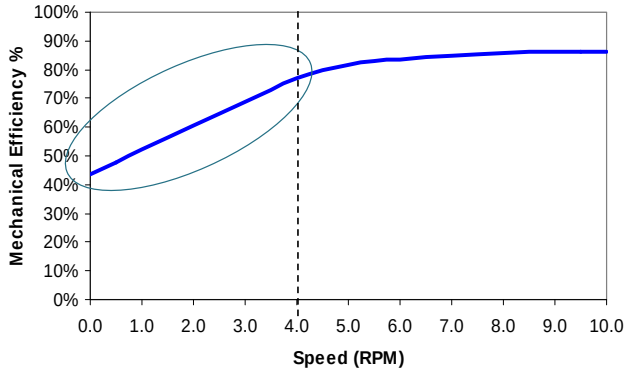

Figure 16. VIS motor suffers low mechanical efficiency at start-up.

The VIS motor mechanical efficiency is mainly affected by the friction forces at two sets of interfaces: (1) the star against rollers and (2) rollers against the ring pockets. The friction

coefficient at each interface is determined by the lubrication regime, motion mode (rolling or sliding), surface textures, and the materials.

The individual and composite roughness values for the star-roller and roller-ring contacts are shown in Table 7. Given the VIS motor operation parameters, the lubricant film thickness and λ-ratio at the star-roller and roller-ring interfaces (both in line contacts) were calculated for three VIS motor operating conditions: 0.1 and 4 rpm at the start-up and 440 rpm at the nominal operation, as shown in Table 8.

Table 7. Roughness of the star, rollers, and ring pockets.

	Star	Roller	Ring
Roughness R_q (μm)	0.406	0.058	0.316
	Star-Roller		Roller-Ring
Composite roughness σ (μm)	0.41		0.32

Table 8. Lubricant film thickness and λ-ratio at the star-roller & roller-ring interfaces

Motor operation condition	Star-Roller		Roller-Ring	
	t (μm)	λ	t (μm)	λ
0.1 rpm @ RT	~0.002	<1 (BL)	~0.02	<1 (BL)
4.0 rpm @ RT	~0.02	<1 (BL)	~0.38	~1 (ML)
440 rpm @ 180 °F	~0.15	<1 (BL)	~2.15	>4 (EHL)

At the start-up, when the star rotation speed is lower than 4 rpm, both the star-roller and roller-ring interfaces are under BL and experience relatively high friction. The high friction at the roller-ring contacts causes a high slip ratio at the star-roller contacts. Therefore, a relatively high torque is required to overcome the BL sliding friction forces (typical coefficient of friction (COF) in the range of 0.05-0.15). This results in a low mechanical efficiency. Reducing the BL COF for the star-roller and/or roller-ring contacts is the key to increase the start-up mechanical efficiency.

When the star rotation speed more than 4 rpm, the star-roller contacts are still under BL (high friction) but the roller-ring contacts transition to ML or EHL (low friction). The nearly free spinning of the rollers in the ring pockets enables a low slip ratio at the star-roller contacts. As a result, a much lower torque is needed to overcome the rolling friction forces (typical COF<0.05) dominated at the star-roller contacts and the ML/EHL sliding friction forces at the roller-ring contacts (typical COF<0.05). This explains why the VIS motor reaches its high mechanical efficiency only after the motor runs at >4 rpm.

The lubrication analyses successfully explained the low-efficiency issue at startup for VIS motors. Furthermore, based on the observation of the BAMC coatings' low friction behavior at in the POD tests (BL), we predicted the BAMC coatings to improve the start-up mechanical efficiency for the VIS motor by allowing rollers rolling on the star at a lower speed and reducing the roller-star sliding friction, as illustrated in Fig. 17. This was later validated in the simulated

bench test, as shown in Fig. 14 and Table 6, and confirmed by dynamometer tests at Eaton Corp., as shown in Fig. ORF18.

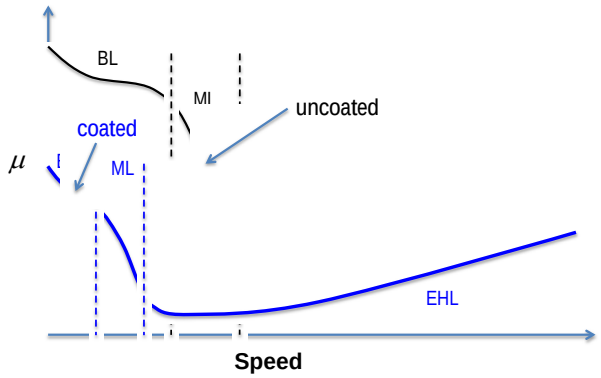

Figure 17. Modeling predicted friction reduction matching the experimental results in Fig. 14.

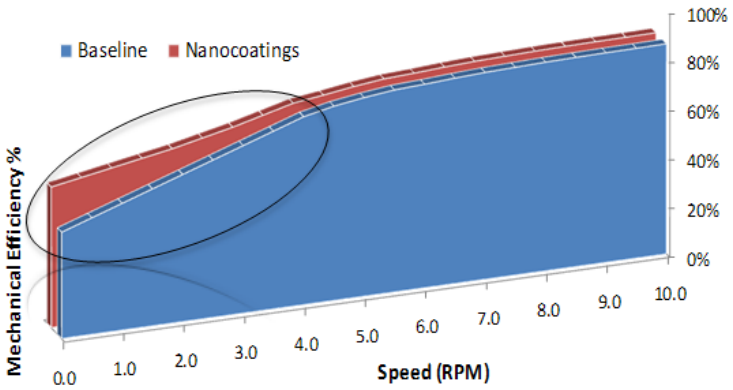

Figure 18. Results of dynamometer tests at Eaton confirmed the efficiency improvement by nanocoatings for VIS motors.

5.0 Subject Inventions and Publications

5.1 Inventions

Patent application filed by Eaton Corporation (2010) C. Higdon, A. Elmoursi, J. Goldsmith, B. Cook, P. Blau, J. Qu, and R. Milner, "Dual material physical vapor deposition targets manufactured from $AlMgB_{14}$ and TiB_2."

5.2 Publications

J. Qu, P.J. Blau, D. Zhu, B.A. Cook, A.A. Elmoursi, "Tribological Characteristics of $AlMgB_{14}$ and Nanocomposite $AlMgB_{14}$-TiB_2 Superhard Coatings,' Proceedings of IJTC2008 STLE/ASME International Joint Tribology Conference, Miami, FL, Oct. 20-22, 2008.

J. Qu, P. J. Blau, A. A. Elmoursi, C. Higdon, and B. A. Cook (2010) $AlMgB_{14}$-TiB_2-C and DLC Coatings to Improve the Startup Efficiency for Hydraulic Motors," presented at the 2010 Annual Meeting of the Society for Tribologists and Lubrication Engineers, Las Vegas, NV, May 16-20, 2010.

B. A. Cook, J. F. Harringa, J. Anderegg, J. Qu, P. J. Blau, and A. A. Elmoursi (2010) Analysis of Wear Mechanisms in Low Friction, Nanocomposite $AlMgB_{14}$-TiB_2 Coatings, submitted to *Surface and Coatings Technology (in press)*

C. Higdon, B. Cook, J. Goldsmith, J. Qu, and P. Blau, et al (2011) "Friction and wear mechanisms in $AlMgB_{14}$-TiB2 nanocoatings," to be presented at the 2011 International Conference on Wear of Materials, and accepted by the journal Wear.

6.0 Commercialization Possibilities

Phase III of the larger program of which this CRADA was a part involved conducting detailed studies of costs and commercialization-related issues. These tasks were undertaken by Eaton Corporation, and indicated the technical and cost feasibility of incorporating AMB nanocomposite coatings in several products in the hydraulic pump line. Penetration into the various markets remains to be established, but there is growing interest within Eaton on applying the coatings to a number of product lines. The final report for the team, prepared by Eaton Corporation, contains a more detailed description of the marketing of the nanocomposite-coated components.

7.0 Plans for Future Collaboration

In the spring of 2010, Eaton Corporation, Ames Laboratory, Oak Ridge National Laboratory, Borg-Warner Morse TEC, and Pratt & Whitney Rocketdyne (PWR), proposed and were awarded an DOE, Industrial Technologies Program, Grand Challenge project titled “Ultracoatings - Enabling energy and power solutions in high contact stress environments through next generation nanocoatings.” It draws on the strong collaborations from the current project to extend coating technology in new directions that are aimed at more severe bearing applications. The description of this new project is as follows:

> “The [new] project seeks to develop a new class of coatings that will enable use of solid lubricants in metal and ceramic-based binders. These coatings will be capable of sustaining higher load-carrying capacity than current state-of-the-art coating compositions, while maintaining low friction. Examples of applications benefiting from such technological advancements would include transmission gears, heavy-duty clutches, aerospace seals and conveyance systems, hydraulics, and automotive supercharger components. The primary technical objective is to develop one or more coating/substrate systems that will sustain a pressure-velocity (PV) product of at least 70,000 (MPa-m/s), consistent with the [chosen] applications.”

8.0 Conclusions

More than four years of tribology studies, surface characterization, and lubricant modeling were conducted in support of the current CRADA. Eaton Corporation and the other team members worked collaboratively to develop both pulsed-laser deposition and physical vapor deposition processes to produce nanocomposite $AlMgB_{14}$/ TiB_2 coatings on several types of hydraulic pump components and cutting tools. ORNL used bench-scale friction and wear tests to evaluate the evolving coating compositions and helped Eaton, Ames, and Greenleaf Corporation to optimize the processing conditions for the low-friction, wear-resistant coatings. The following tests provided useful information:

- Coating thickness and microindentation hardness tests
- Lubricated unidirectional sliding pin-on-disk tests using steel as the counterface
- Lubricated reciprocating sliding pin-on-flat tests using steel as the counterface
- Reciprocating sliding pump piston ring on bore tests
- Reciprocating rolling/sliding roller-in-groove tests

Depending on the coating thickness and the addition of carbon films, the running-in behavior and hence, the long-term friction coefficients could be reduced to an impressive low of 0.03 or less. Results of ORNL laboratory tests were in many cases consistent with trends observed during full-scale hydraulic pump tests at Eaton's Eden Prairie test facility. Two different pumping fluids that varied in lubricity were studied. It was found that the friction and wear behavior of one of the fluids, originally believed to be less lubricative, was in fact better than expected, and that prompted a reexamination of the need to derate pumps for service with that less lubricative fluid.

Published lubrication models from the literature were used to calculate film thickness and develop explanations of the tendency for rollers to slip or roll. That affected the friction and efficiency of the components. A map-like representation of frictional operating conditions for valve-in-star motors was developed and well-received by Eaton engineers.

During the course of the work, market forces affected which products were most likely to be equipped with the nanocomposite coating, but several divisions of Eaton Corporation found sufficiently interesting results to pursue further roads to commercialization.

9.0 References

1. Y. Tian, A. F. Bostawros, C. C. H. Lo, A. P. Constant, A. M. Russel, and B. A. Cook (2003) “Superhard self-lubricating AlMgB14 films for microelectromechanical devices,” Appl. Phys. Letters, Vol. 83 (14) pp. 1-3.

2. B. J. Hamrock and D. Dowson (1981) Ball bearing lubrication: The elastohydrodynamics of elliptical contacts, Wiley-Interscience Pub., New York, 409 pp.

……

10.0 Symbols and Nomenclature

Symbols

α	viscosity pressure coefficient
η_o	atmospheric absolute viscosity
λ	film thickness to composite surface roughness ratio
μ	friction coefficient (see also COF)
$\nu_{1,2}$	in film thickness calculations, the dimensionless Poisson's ratio of body 1 or 2
σ	square root of the sums of the squares of the *Rq* of two opposing surfaces
σ_n	*Rq* of surface designated as subscript n
C	geometric constant used in hardness testing
D	length of a hardness impression left when the indenter is removed
d_i	in thickness measurement using ball cratering, the inner dimple diameter
d_o	in thickness measurement using ball cratering, the outer dimple diameter
E	in film thickness calculations, the ellipticity of the contact
E'	in film thickness calculations, the composite elastic modulus for both surfaces
$E_{1,2}$	in film thickness calculations, the elastic modulus of surfaces 1 or 2
G	in film thickness calculations, the bulk elastic modulus
H	indentation hardness (generic)
h	lubricant film thickness
HK	Knoop microindentation hardness
h_{line}	film thickness in line contact between bodies
h_{point}	film thickness in point contact between bodies
HV	Vickers microindentation hardness
P	applied (normal) load (also designated as *w* in film thickness calculations)
R	in thickness measurement using ball-cratering, the radius of the spinning ball
Ra	arithmetic average surface roughness
Rq	root mean square surface roughness
$R_{x, y}$	in film thickness calculations, the effective radii of curved surfaces in contact in x and y directions
t	coating thickness
U	in film thickness calculations, the dimensionless speed
W	in film thickness calculations, the dimensionless load
w	in film thickness calculations, the normal load
z	direction perpendicular to the plane of a flat surface (height or depth)

Nomenclature

AMB	a compound of AlMgB14 - the matrix for NAMB nanocomposite coatings
BAM	used interchaneably with AMB by the team members (see also AMB)
BAMC	a BAM film containing a thin carbon layer on the surface
BL	the boundary lubrication regime of liquid lubrication

Btu	British thermal unit - customary unit for the energy required to raise a pound of water 1 degree Fahrenheit at the temperature of highest liquid density
COF	alternative abbreviation (to Greek mu) for the coefficient of friction
CRADA	Cooperative Research and Development Agreement
DLC	diamond-like-carbon, a thin hard film used for comparison in this study
EBxxxx	designation for coatings produced at Eaton Corporation during the project
EHL	elasto-hydrodynamic lubrication regime of liquid lubrication
ER	elastic recovery after indenting a surface
HK	Knoop microindentation hardness number
HV	Vickers microindentation hardness number
ITP	Department of Energy IndustrialTechnologies Program
M2	a tool steel alloy used as a substrate for coating studies
ML	mixed or partial film lubrication regime that falls between BL and EHL
NAMB	nano-composite material with the formula AlMgB14
ORNL	Oak Ridge National Laboratory
PLD	pulsed laser deposition, method of coating used by Ames Lab
POD	pin-on-disk tribotest geometry
PVD	physical vapor deposition
RPOF	reciprocating pin-on-flat specimen tribotest geometry
RT	room temperature
TSA	Tribo-System Analysis to define a friction or wear-critical application
UC	un-coated base material, used as an abbreviation in some tables and plots
VEOR	vane-edge sliding on ring tribotest geometry
VIS	valve-in-star type hydraulic pump design
WC	tungsten carbide (also WC-Co, referring to WC with a cobalt binder)
WR	wear rate (volume removed per unit sliding distance per unit applied load)